Dissolution of Oxygen Precipitate Nuclei in n-Type CZ-Si Wafers to Improve Their Material Quality: Experimental Results

Bhushan Sopori, Prakash Basnyat, Srinivas Devayajanam, Teh Tan, Ajay Upadhyaya, Keith Tate, Ajeet Rohatgi, and Han Xu

***Abstract*—We present experimental results which show that oxygen-related precipitate nuclei (OPN) present in p-doped, n-type, Czochralski wafers can be dissolved using a flash-annealing process, yielding very high quality wafers for high-efficiency solar cells. Flash annealing consists of heating a wafer in an optical furnace to temperature between 1150 and 1250 °C for a short time. This process produces a large increase in the minority carrier lifetime (MCLT) and homogenizes each wafer. We have tested wafers from different axial locations of two ingots. All wafers reach nearly the same high value of MCLT. The OPN dissolution is confirmed by oxygen analysis using Fourier transform infrared spectra and injection-level dependence of MCLT.**

***Index Terms*—Charge carrier lifetime, chemical etching, optical furnace, silicon solar cells, spatial diversity.**

I. Introduction

CURRENTLY, n-type (p-doped) Czochralski (CZ)-Si wafers are available with a long (few milliseconds) minority carrier lifetime (MCLT) in the as-grown state. This important advancement in wafer technology has primarily been made possible by using very high quality poly feedstock and maintaining cleanliness of the crystal growth equipment, which enables growth of low-Fe and low-C Si ingots. Although the MCLT of n-type Si is considerably less sensitive to Fe contamination, as compared with the p-type Si, having MCLT of a few milliseconds still requires low contamination levels of Fe: typically about (or less than) 10^{11} cm^{-3}. In spite of this advancement, there remain two major problems that still need to be solved before n-type wafers can be commercially used (without a preselection of wafers) by the majority of solar companies. These problems are the following: 1) A CZ-grown ingot shows a large variation in the material quality of wafers taken along the axial direction (which is also discussed further in this paper). Consequently, only a limited fraction of wafers can be used for very high efficiency cell fabrication, reducing the yield (number of useable wafers per ingot length) of the ingot; and 2) it is a common experience that many n-type wafers, particularly those with moderate-to-high O and C content, develop swirl defects during cell fabrication, with a concomitant degradation in MCLT [1]–[3]. Typically, the MCLT can be reduced from several milliseconds to a few hundred microseconds, thus severely limiting the cell efficiency. Interestingly, both of these problems happen to have the same origin—they both are related to the presence of oxygen precipitate nuclei (OPN) in the wafers.

The OPN are embryos in the ingot that can lead to oxygen precipitation during device fabrication. They are formed by the interaction of point defects and impurities like O and C during crystal growth [4]–[6]. A great deal of work has been done in the area of O-related nucleation and precipitation by researchers who studied internal gettering, as used in microelectronic devices [7], [8]. That work has shown that OPN undergo Ostwald ripening during extended high-temperature processing (such as B diffusion/drive-in and oxidation), producing SiO_2 precipitates in the form of swirl defects [1], [9], [10]. Oxygen precipitation is influenced by the injection of point defects that may be generated during high-temperature processing and is accompanied by generation of stacking faults and dislocations, concomitantly greatly increasing carrier recombination [11], [12].

Hence, it can be concluded that OPN are a major problem that leads to degradation of wafer quality during cell fabrication. Fortunately, there is a well-known solution to this—dissolving the OPN prior to B diffusion/oxidation or cell fabrication. This concept (which is also called Tabula Rasa treatment) has been used in microelectronics to control point defect distributions in the wafer for optimizing internal gettering. This concept has been applied for decades to dissolve grown-in OPN for internal gettering studies [13], [14]. In particular, first, wafers are given a high-temperature annealing step (typically for a few minutes to several hours) to dissolve grown-in OPN. Next, wafers are given a low-temperature step to homogeneously generate OPN of desired size, followed by a high-temperature precipitation anneal. Recently, the high-temperature step has also been done using rapid thermal anneal (RTA) or RTA-like processes [15], [16]. However, in these low-high temperature annealing studies, very little attention was paid to MCLT and was rarely reported. This is because bulk MCLT is not of primary importance for microelectronic devices. Recently, this method (which is also called

Manuscript received September 11, 2016; revised October 13, 2016; accepted October 17, 2016. Date of publication December 5, 2016; date of current version December 20, 2016. This work was supported by in part by Bay Area PV Consortium and Photovoltaic Manufacturing Consortium.

B. Sopori, P. Basnyat, and S. Devayajanam are with the National Renewable Energy Laboratory, Golden, CO 80401 USA (e-mail: Bhushan.Sopori@nrel.gov; Prakash.basnyat@nrel.gov; Srinivas.Devayajanam@nrel.gov).

T. Tan is with Duke University, Durham, NC 27708 USA (e-mail: ttan@duke.edu).

A. Upadhyaya, K. Tate, and A. Rohatgi are with Georgia Institute of Technology, Atlanta, GA 30332 USA (e-mail: ajay.upadhyaya@ece.gatech.edu; keith.tate@ece.gatech.edu; ajeet.rohatgi@ece.gatech.edu).

H. Xu is with GT Advanced Technologies, Merrimack, NH 03054 USA (e-mail: han.xu@gtat.com).

Color versions of one or more of the figures in this paper are available online at http://ieeexplore.ieee.org.

Digital Object Identifier 10.1109/JPHOTOV.2016.2621345

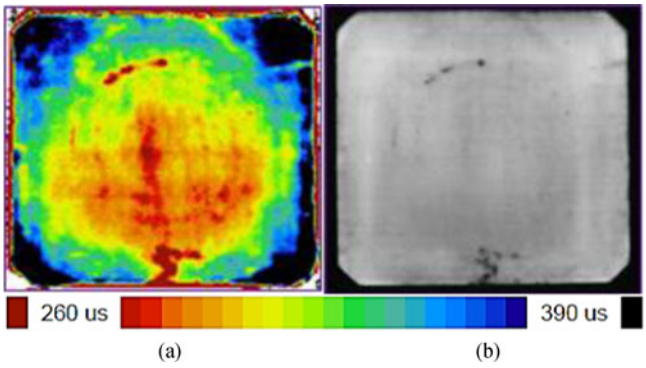

Fig. 1. (a) MCLT map and (b) PL map of low-quality ingot material showing swirl defect formation in the tang end of ingot B.

Tabula Rasa treatment) has also been proposed for photovoltaic (PV) Si wafers by several researchers, with no verification [17]–[19]. However, some researchers have found that Tabula Rasa treatment indeed moderated the degradation of MCLT wafers that went through thermal treatments like B diffusion and oxidation [12]. However, we believe that to date, direct evidence of improving the MCLT of low-performing wafers of an ingot to that of the best wafers by a single annealing step has not been published. Although this solution is conceptually simple, there are numerous hurdles to apply a very high temperature process step to high-quality wafers, and that a commercially compatible process for OPN dissolution is not yet available. In particular, it is extremely important that the processing itself should protect wafer from impurity infusion and prevent any defect generation in the wafer.

In this paper, we show that "flash annealing" (FA) is able to dissolve these precipitate nuclei and our preliminary results are very promising. We show that this single-step process improves the MCLT of all wafers—specifically those with higher OPN density (from the tang end of the ingots) are improved to values that correspond to best wafers in the ingots.

II. Oxygen Precipitate Nuclei and O Precipitation

OPN are formed during the crystal growth itself because CZ growth using quartz crucible provides high concentration of oxygen to the melt and to the solidifying crystal [4], [20], [21]. Formation of OPN occurs during cooldown part of the crystal growth, typically when the ingot is in the temperature range of 800–1000 °C, by the interaction of point defects and O. Other impurities such as C and B can enhance the OPN formation [22], [23]. In most cases, OPN are very small in size, typically range in size of 25–200 Å (depending on the temperature profile which the ingot undergoes) and can be seen only by a transmission electron microscope. However, if concentrations of both O and C are high in parts of the crystal, the embryo size can be slightly larger and a partial segregation can occur at the swirl (vacancy) pattern. In such a case, a pattern can be observed on wafers (typically near the tang end of the crystal) with several techniques. For example, delineation of ingrown pattern of OPN by MCLT and photoluminescence (PL) mapping is shown in Fig. 1(a) and (b), respectively. It is clear from Fig. 1 that the presence of OPN can degrade the MCLT of the wafers. More severe degradation occurs when OPN actually form O precipitates.

We should point out the MCLT and PL maps shown in Fig. 1 are done using iodine–ethanol (I–E) passivation, and the wafers are quite thin (about 160 μm) with rough surfaces (as described later in this paper). Consequently, surface passivation leads to rather high S_{eff} in the range of 5–8 cm/s.

OPN grow into oxygen precipitates during extended high-temperature processing (at temperatures around 950–1100 °C). Precipitation can be further enhanced by B diffusion/drive-in and oxidation—processes that inject Si interstitials into the bulk of the wafer. The resultant SiO_2 precipitates cause very high carrier recombination, lowering bulk lifetime (τ_b), and increasing junction leakage current of the solar cell [24].

Si-PV wafer suppliers have attempted to solve the problem in the crystal growth (by trying to lower O content, reducing C content, and controlling point defect distributions). However, it has not been successful to date. However, this problem can be solved at wafer level without adding a significant cost to the wafer. Wafer-level processing is very efficient because point defects can be rapidly driven to the surfaces, which act as their sinks. Thus, a new defect equilibrium can be set in a short period of time.

III. Flash Annealing and a Brief Description of Optical Furnace

Nucleation and growth theory suggests that OPN can be dissolved at high temperatures—temperatures where the nuclei size is below the critical size [13], [24], [25]. Hence, if a wafer is heated to a high temperature, the OPN will shrink and dissolve [18], [19]. A detailed discussion of the dissolution process will be given elsewhere [26]. Here, we will only qualitatively establish operating conditions for the precipitate dissolution for cases of interest to solar cell wafers. To do that, we will assume that the size of the largest OPN is $\sim$ 100 Å. This is quite reasonable from the data published in the literature [5], [27]. For this critical size, we need to estimate process temperature and time. The required process temperature can be estimated from the results of [22] and [28], suggesting process temperature to be in the range of 1150–1250 °C. Another important parameter is time needed to dissolve OPN. Because dissolution time depends on the precipitate size, temperature, and the difference between oxygen concentration in the wafer and the equilibrium solubility at temperature T, an optimum time duration can be difficult to predict. However, it is known that larger size precipitates can be dissolved in thermally pretreated samples using the so-called low–high treatment by heating to 1200 °C for a short period of time [15], [22]. We have performed some detailed experiments and have selected two process conditions, which will be illustrated in the next section.

In the meantime, we will assume that OPN can be dissolved with process times that can be quite short ($\sim$ 2–3 min). Process times can be further reduced by simulating conditions for injecting Si interstitials, which favor the reverse reaction based on the increased volume upon oxidation, resulting in kick-out of Si interstitials (I_{si}):

$$\text{Si} + 2O_i \leftrightarrow \text{SiO}_2 + \text{I}_{\text{si}}.$$

This reaction suggests that the dissolution process will be favored in oxygen ambient, which injects interstitials from the surface. Because annealing must be done at a very high temperature, there are stringent requirements for cleanliness and temperature uniformity. The furnace cleanliness must be compatible with processing wafers of a several-millisecond MCLT. Likewise, a high degree of temperature uniformity is needed to prevent any defect generation (and, in an extreme case, prevent wafer shattering). These requirements are easily met in optical processing furnaces (OPF) developed by the National Renewable Energy Laboratory, which is described briefly in the following.

OPFs are single-wafer processors that use a square optical cavity of reflecting walls. A quartz muffle of rectangular cross section is located within the cavity to hold a square wafer. A distributed light source of multiple zones, having a geometry that produces adjustable optical flux incident on the wafer, is used. The distribution of the flux can be adjusted by controlling the emission from each zone to create a flux distribution on the wafer that produces a highly uniform temperature (about ± 1 °C) over 156 mm $\times$ 156 mm wafer. The flow of gases is distributed through the muffle. Because the quartz muffle has very low optical absorption, its temperature remains well below 200 °C, even when the wafer is processed at temperatures above 1200 °C. This design is favorable for intrinsic clean processing, where any residual impurities from the hot wafer surface are driven toward the cooler walls of the muffle and carried away by the flowing process-gas stream (thermophoresis). Additional cleanliness is achieved by photophoresis: a mechanism where small particles from the wafer surface are knocked by the momentum of a very large flux density. This intrinsic self-cleaning ability of the furnace obviates need for costly processing schedules such as Trans-LC (HCl cleaning) and clean room operation. All results of FA presented in this paper correspond to processing without HCl cleaning of the quartz parts. Other features of OPFs are the following: have no active cooling, are highly energy efficient, have capability of adjusting the temperature uniformity, and are designed for long lamp longevity (lifetimes $>>$ 1000 h).

IV. Experimental Details

Wafers were chosen from two n-type ingots, with nominal resistivity of 1–2 $\Omega\cdot$cm—ingot A and B, with some specific properties. Groups of wafers (G1–G4) were taken from four different locations, as illustrated in Fig. 2. The characteristics of the ingots, in terms of oxygen, carbon concentrations, and MCLT (measured on the ingot using Sinton ingot tool, BCT-400, at an injection level of 1e15 cm^{-3}), are shown in Table I. Wafers were diamond wire sawn with nominal thickness of 190 μm. The surface damage was removed by etching in HNO_3:HF:CH_3COOH::1:1:5 solution, as described in previous papers [29]. As discussed in this reference, this etch is basically an isotropic etch but has some sensitivity to damage. Typically, 6–8 μm were removed from each surface, resulting in wafers of about 170-μm thickness. Consequently, the resultant wafer surfaces remain rather rough. Representative wafers from each group were characterized by injection-dependent lifetime and

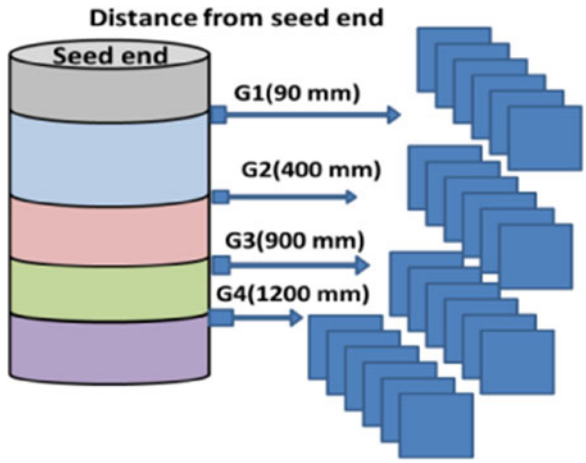

Fig. 2. Schematic of wafers used from each ingot. G$_i$ indicates group #, and numbers in parenthesis indicate distance from the seed end. Oxygen and carbon concentrations are listed for both the ingots in Table I.

TABLE I
Oxygen, Carbon, and Bulk MCLT Measured at Different Parts of the Ingots Used in This Study

Wafer group	Ingot A			Ingot B		
	O (ppma)	C (ppma)	MCLT (μs) (ingot)	O (ppma)	C (ppma)	MCLT (μs) (ingot)
G1	15.1	0.46	4765	15.9	0.98	1825
G2	12.4	0.49	4992	13.9	1.05	1701
G3	12.6	0.53	4043	14.0	1.37	1478
G4	12.6	0.75	3201	13.8	1.04	1304

O and C measurements [30], [31]. It is seen that ingot A has lower C and O concentrations and higher MCLT over the entire ingot. This feature allows us to compare the effect of FA on slightly different material quality.

To measure the MCLT, damage etched wafers were first cleaned in piranha ($2H_2SO_4$: H_2O_2) at 80 °C for 20 min, rinsed in 18 MΩ deionized water, and dried. Each wafer was then dipped in diluted HF, dried, and placed in polyethylene ziplock bag. Next, few drops of I–E solution (0.1 molar) were squirted on each surface and the bag was sealed. The wafer in I–E solution was immediately measured with Sinton tool WCT100 (transient mode). The Sinton lifetime was measured typically in two places over each wafer—on the top-middle and left-middle. Following the lifetime measurement, wafers were mapped with μ-PCD tool (Semilab WT 2000). This procedure ensured that there was minimum reduction in S_{eff} (due to I–E degradation) during Sinton lifetime measurements, enabling us to acquire the highest possible values of MCLT with least degradation effect.

It also provided a time gap to stabilize the I–E-Si system and reduce its rate of degradation during MCLT mapping (which takes 20–30 min). This would give meaningful lifetime maps (even though the MCLT values are lower).

Each group of wafers was flash-annealed under two slightly different process conditions (Processes A and B). A typical

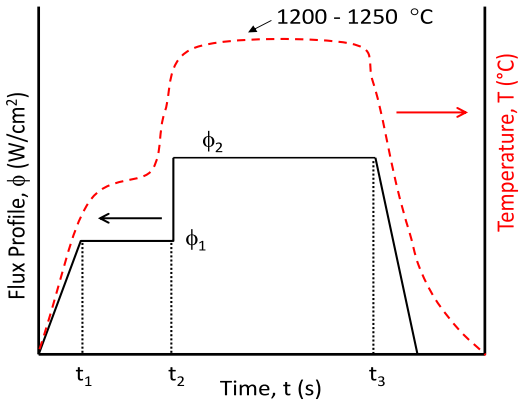

Fig. 3. Typical flux and temperature profiles used in our OPF during an FA process. Note that segment $(t_2 - t_3)$ for process B is 5 s longer than that for process A.

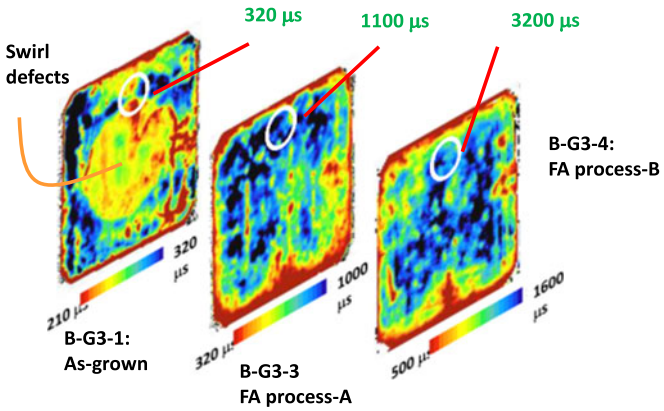

Fig. 4. MCLT maps of (left) unprocessed, (middle) shorter flash annealed, and (right) longer flash annealed sequential wafers.

optical flux profile of an FA process is shown in Fig. 3. This process involves two segments: segment 1 that raises the optical flux linearly to a level ϕ_1 and holds it during time t_1 to t_2; and segment 2 that raises the optical flux abruptly to a level ϕ_2 and holds it during time t_2 to t_3. The corresponding temperature profiles are also illustrated in Fig. 3. The entire process takes less than 2 min. Process B has second segment, $(t_2$–$t_3)$, which is 5 s longer, while all other parameters are same. The entire process is done with oxygen gas ambient. Although our optical furnaces have trans-1, 2-dichloroethylene capability, there was no HCl type of cleaning used in this furnace. This is simply to show that our process is commercially compatible and low cost.

V. Results

First, we show the effect of FA on wafers from ingot B (a lower quality), taken from near-tang end (B-G3). Fig. 4 compares MCLT maps of three sequential wafers (156 mm × 156 mm). The wafer on the left, i.e., B-G3-1, is unprocessed and displays a swirl pattern of OPN. The color legend shows the highest MCLT to be 320 μs. Also shown on the top (region marked by white circle) is the maximum value of MCLT measured by Sinton's wafer-lifetime tool (WCT-100), which is also 320 μs. Fig. 4 also

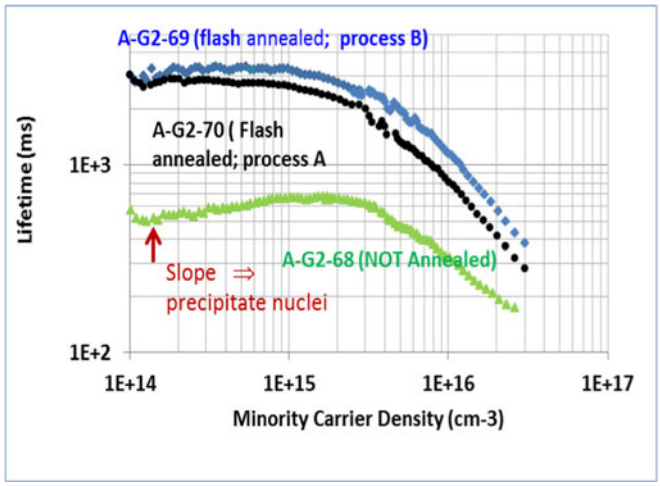

Fig. 5. Comparison of results of two FA processes, i.e., A and B, on wafers from ingot A. For reference, the lifetime plot of unannealed wafer is also shown.

shows MCLT maps of two flash-annealed wafers. The middle wafer was annealed with process A, while the wafer on the right was annealed with process B.

An important feature can be clearly seen in both processed wafers—the swirl pattern has been eliminated by FA. Furthermore, for the middle wafer (process A), the maximum value in the MCLT map has increased to 1 ms, while the maximum MCLT at the top of the wafer with Sinton tool is now 1.1 ms. For the wafer on the right-hand side (process B), the MCLT map shows further increase to a maximum value of 1.6 ms, while Sinton tool shows an increase to 3.2 ms. These results clearly show precipitate dissolution and its dependence on the process time.

It should be noted that the MCLTs of FA wafers from ingot B have increased above the ingot values (as seen in Table I) and are approaching that of ingot A. We should mention that the thickness of all the wafers shown in Fig. 4 is about the same (∼155 μm). However, their surfaces are quite rough, giving rather large S_{eff}, which we have estimated to be in 5–7 cm/s range. This estimation is done in two ways: 1) comparing lifetimes from ingot with the lifetime we obtain from wafers of known thickness and 2) measuring MCLT of adjacent wafers but etched to different thicknesses.

Let us look at the effect of FA on the MCLT plot (injection-level dependence). Fig. 5 shows these plots for three wafers from group A-G2. Wafer # A-G2-68 is unannealed; A-G2-70 is annealed with profile A, while A-G2-69 is annealed with process B. Two important observations from Fig. 5 are the following: 1) The maximum lifetime increases from about 700 μs for unprocessed wafer to 3 ms for process A and 3.2 ms for process B (before Auger recombination takes over); and 2) the MCLT of A-G2-68 increases with injection level (up to 2×10^{15} cm^{-3}). On the other hand, the plots for annealed wafers are near ideal and do not show low-level injection dependence. Because we do not expect the Fe concentration to change during FA, this implies that the injection-level dependence of unprocessed wafer is related to the recombination associated with OPN.

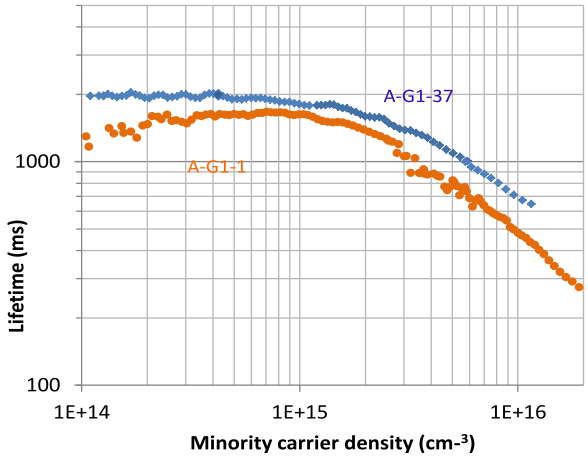

Fig. 6. Comparison of FA and unannealed wafers from ingot A. The MCLT remains almost unchanged by FA.

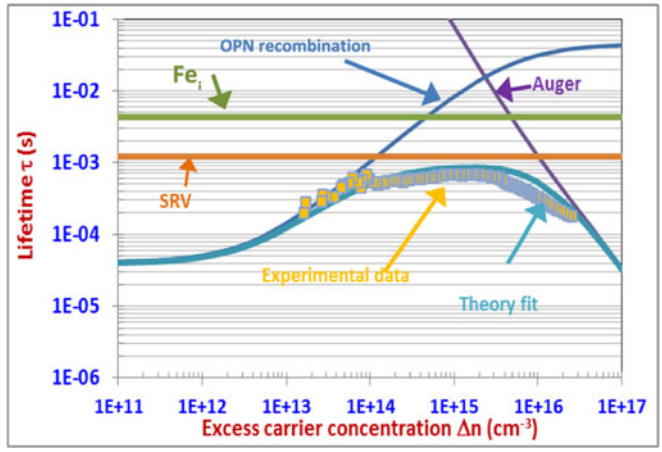

Fig. 7. Comparison of theoretical and experimental MCLT plots with the oxygen precipitates. Lifetime-limiting parameters and their effect on the lifetime and the injection-level dependence are also shown. The fitted data correspond to $E_c - E_t = 0.2$ eV and $\sigma_n = 1 \times 10^{-19}$ cm^2.

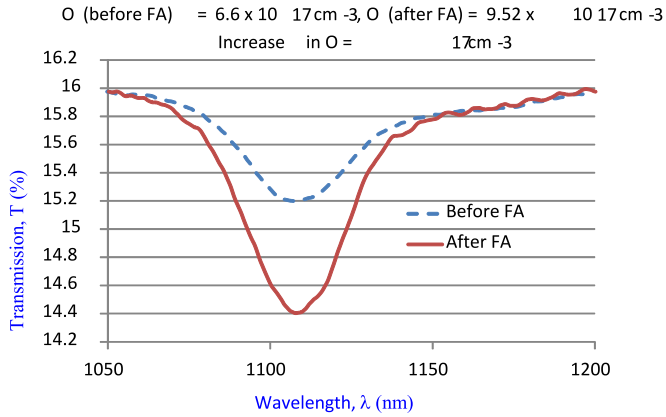

Fig. 8. FTIR spectra before and after FA: dashed blue, unannealed, and solid red, flash annealed, showing that dissolution of OPN is accompanied by increase in dissolved O.

Now, we consider MCLT plots of higher quality ingot A, before and after FA. Fig. 6 compares MCLT versus injection level of wafers A-G1-1(unannealed) and A-G1-37 (FA). These wafers were not of the same thickness. AG1-1 was only 100 μm in thickness, while AG-1-37 was 160 μm thick. Keeping this in mind, it is clear that FA does not affect MCLT to any significant level. It is worth noting that A-G1-1 does display some injection-level dependence, indicating the presence of some OPN. Furthermore, because the bulk MCLT of the wafers is known from the ingot measurement, we can estimate the S_{eff} for this wafer to be about 4–6 cm/s (within uncertainty of the thickness uniformity and other errors in making MCLT measurement).

To further support the argument that the injection-level dependence of unannealed wafer comes from OPN, we have modeled unprocessed wafer lifetime using two-trap model (Fe$_i$ and OPN) and the following well-known relationship:

$$1/\tau_{\text{eff}} = 1/\tau_{\text{SRHO}} + 1/\tau_{\text{Fe}} + 1/\tau_{\text{SR}} + 1/\tau_{\text{Aug}}$$

where τ_{Fe}, τ_{SRHO}, τ_{SR}, and τ_{Aug} correspond to lifetimes associated with Fe, OPN, surface recombination, and Auger, respectively. To perform these calculations, we have used standard formulas and data from the literature for energy levels and capture cross sections of Fe and Auger coefficients [32]. The expression for τ_{SRHO} is very similar to that of τ_{Fe}. We have also used a surface recombination value for I–E-passivated Si wafer surface as 7 cm/s, which was determined from known bulk lifetime of the wafers (as measured on the ingot). Fig. 7 shows results of our calculations, where we have shown measured τ_{eff} data and the best (visual) fit of calculated τ_{eff} to the measured data. This fit yields the following values: OPN trap level, $E_t = E_c - 0.2$ eV with electron capture coefficient of 10^{-19} cm^2; Fe$_i$ concentration of 1.6×10^{11} cm^{-3}, and the OPN density of 2×10^{13} cm^{-3}. The objective of this exercise is only to obtain a value of OPN density, which releases O upon annealing and to compare the increase in dissolved oxygen with actual measurement. Hence, we have sought the best fit utilizing available information on possible values of trap energy.

The Fe concentration matches τ values published in [32] and [33]. They also match the values provided by the vendor. It may be noted that Fe and surface recombination velocity (SRV) have very weak injection-level dependence. Because we expect Fe concentration and SRV to be about the same for unannealed and annealed wafers, a fit to the MCLT curve of annealed wafer allowed us to determine the Fe concentration. However, SRV was determined from bulk MCLT and the wafer MCLT, knowing the wafer thickness. We would like to point out that the objective of the above fit is to estimate the concentration of recombination centers and to validate that these centers originate from OPN.

We would like to mention that injection-level dependence of annealed wafers (see Fig. 5) can be generated using the Fe concentration of 1.6×10^{11} cm^{-3}, the trap density = 0, and the SRV value of 2 cm/s. The lower value of SRV is compatible with the fact that S_{eff} of annealed wafers is lower because surface/near-surface region is devoid of any defects due to OPN.

Now, we can check if OPN density is reasonable. To do that, we will first determine the increase in the dissolved O concentration due to FA. Fig. 8 shows Fourier transform infrared (FTIR) transmission spectrum corresponding to O peaks (1107 cm^{-1}) before and after FA. From these data, and using the

new ASTM (ASTMF121-83) published calibration coefficient of 2.45×10^{17} cm^{-2}, the calculated increase in O concentration was determined to be 2.9×10^{17} cm^{-3}. We should mention that in principle, it is possible to corroborate increase in dissolved oxygen with a decrease in the precipitated oxygen (1230 cm^{-1}) peak height. However, because our samples are thin, we were not able to detect the precipitated O peaks. It will require internal multireflection technique to do those measurements.

From the measured increase in dissolved O concentration, we can determine OPN density ($N_{\rm OPN}$), using the expression given in [10]:

$$\left[4/3 \cdot \pi r_0^3\right] \cdot C_p \cdot N_{\rm OPN} = [{\rm O}_i]_i - [{\rm O}_i]_f$$

where r_0 = average radius of OPN, $C_{\rm p}$ = atomic density of oxygen in OPN= 4.5×10^{22} cm^{-3}, and $N_{\rm OPN}$ = average OPN density. Here, we assume OPN to be spherical SiO_2 particles of 100 Å in diameter. This expression yields $N_{\rm OPN} = 2 \times 10^{13}$ cm^{-3}. We should point out that we have not made any attempts to consider effects of SiO_2 being under compression in the Si lattice.

We can now use $N_{\rm OPN}$ to estimate density of traps associated with the trap level E_t. The traps are assumed to be similar to those at the Si–SiO_2 interface (without H annealing) [34], [35]. To determine the trap density, we calculate the total Si–SiO_2 area of each OPN of 50 Å in radius to be $\sim 3 \times 10^{-12}$ cm^2. Using typical trap density in the range of 5×10^{11} cm^{-2} to 10^{-12} cm^{-2}, trap density associated with $N_{\rm OPN}$ in the range of 2×10^{13} to 6×10^{13} cm^{-2}. We believe that these qualitative agreements (within an order of magnitude) are quite sufficient to show the validity of the recombination mechanism due to OPN.

VI. Discussion/Conclusion

We have shown that FA can be performed in optical furnaces, without any indiffusion of impurities, and the MCLT can be greatly improved by this step alone. FA was performed on a large number of wafers from two different ingots (low-Fe content). In all cases, the MCLT increased from 300–700 μs range to 2–3.2 ms range. We also show that FA resulted in MCLT of wafers from both ingots to be about the same after FA. We have also shown that the increase in MCLT is caused by OPN dissolution. We would like to point out that the MCLT reported here is the effective lifetime on the wafers that have thickness of about 150 μm (and even thinner in some cases). However, the measurements before and after annealing are very accurate and comparable because the wafer thickness and preparation procedure are exactly the same.

We have shown that the best fit to measured lifetime data, using a two-trap model, gives a reasonable trap level at E_c – 0.2 eV. Although many different levels have been reported in the literature, they do not necessarily correspond to OPN but are more characteristic of large oxygen precipitates. Our values are, however, close to those reported in an excellent paper of Hwang and Schroder [36]. They have reported possibility of a range of σ_n between 10^{-16} and 10^{-18} cm^2. However, their wafers had MCLT less than 10 μs, which had other impurities that resulted in larger effective capture cross section.

We would also like to point out that we have identified some of the nonuniformities (as seen in Fig. 2). Many of these are from wafer handling and have been corrected to obtain more uniform lifetime and PL maps after annealing. We have performed B and P diffusion on FA wafers and verified that the improvement in the MCLT is maintained. Cell data are not available at this time.

Acknowledgment

The authors would like to thank Y. Liu and N. M. Ravindra for performing FTIR measurements.

References

[1] B. Sopori *et al.*, "Bulk defect generation during B-diffusion and oxidation of CZ wafers: Mechanism for degrading solar cell performance," in *Proc. 40th IEEE Photovoltaic Spec. Conf.*, 2014, pp. 719–723.
[2] P. Cousins and J. Cotter, "Influence of diffusion induced dislocations on high efficiency silicon solar cells," *IEEE Trans. Electron Devices*, vol. 53, no. 3, pp. 457–464, Mar. 2006.
[3] M. Kessler, T. Ohrdes, B. Wolpensinger, R. Bock, and Nils Harder, "Characterization and implications of boron rich layer resulting from open-tube liquid source BBr3boron diffusion processes," in *Proc. 34th IEEE Photovoltaic Spec. Conf.*, 2009, pp. 1556–1561.
[4] H. Furuya, I. Suzuki, Y. Shimanuki, and K. Murai, "Formation of nuclei of oxygen precipitates in CZ silicon crystal during crystal growth process," *J. Electrochem. Soc.*, vol. 135, no. 3, pp. 677–682, 1988.
[5] F. Shimura, H. Tsuya, and T. Kawamura, "Precipitation and redistribution of oxygen in Czockralski-grown silicon," *Appl. Phys. Lett.*, vol. 37, no. 5, pp. 483–486, Sep. 1, 1980.
[6] J. Vanhellemont, E. Smoen, A. Kaniava, M. Libenzy, and C. Claeys, "Impact of oxygen related extended defects in silicon diaode characteristics," *J. Appl. Phys.*, vol. 77, no. 11, pp. 5669–5676, 1995.
[7] M. Kulkarni, "Defect dynamics in the presence of oxygen in growing Czocharlski silicon crystals," *J. Cryst. Growth*, vol. 303, pp. 438–448, 2007.
[8] H. Zimmermann and R. Falster, "Investigation of the nucleation of oxygen precipitates in Czochralski silicon at an early stage," *Appl. Phys. Lett.*, vol. 60, no. 26, 1990, Art. no. 3250.
[9] A. Bourret, J. Thibault-Desseaux, and D. N. Seidman, "Early stages of oxygen segregation and precipitation in silicon," *J. Appl. Phys.*, vol. 55, no. 4, 1984, Art. no. 825.
[10] V. V. Voronkov and R. Falster, "Strain-induced transformation of amorphous spherical precipitates to platelets: Applications to oxide precipitates in silicon," *J. Appl. Phys.*, vol. 89, no. 11, 2001, Art. no. 5965.
[11] I. Kolevatov *et al.*, "Oxygen-related defects: Minority carrier lifetime killers in n-type Czochralski silicon wafers for solar cell application," *Phys. Status Solidi C*, vol. 12, no. 8, pp. 1108–1110, 2015.
[12] D. Walter, B. Lim, R. Falster, J. Binns, and J. Schmidt, "Understanding lifetime degradation in Czochralski-grown N-type silicon wafer after high-temperature processing," in *Proc. 28th Eur. Photovoltaic Sol. Energy Conf. Exhib.*, Paris, France, Sep. 30–Oct. 4, 2013, pp. 699–702.
[13] R. Falster, M. Cornara, D. Gambaro, M. Olmo, and M. Pagani, "Effect of high temperature pre-anneal on oxygen precipitates nucleation kinetics in Si," *Solid State Phenomena*, vols. 57/58, pp. 123–128, 1997.
[14] M. Meduna, O. Caha, and J. Burski, "Studies of influence of high temperature preannealing on oxygen precipitation in CZ Si wafers," *J. Cryst. Growth*, vol. 348, pp. 53–59, 2012.
[15] F. Shimura, *Semiconductor Silicon Crystal Technology*. San Diego, CA, USA: Academic, 1989, pp. 361–367.
[16] M. Meduna, O. Caha,, J. Kubena, and J. Burski, "Homogenization of CZ SI wafers by tabula rasa annealing," *Phys. B*, vol. 404, pp. 4637–4640, 2009.
[17] R. J. Falster, "Non-oxygen precipitating Czochralski silicon wafers," U.S. Patent 6 336 968B1, Jan. 8, 2002.
[18] J. P. DeLuca, "Thermal treatment of silicon wafers useful for photovoltaic applications," U.S. Patent US2012/0 260 989A1, Oct. 18, 2012.
[19] F. Shimura, "Redissolution of precipitated oxygen in Czochralski grown silicon wafers," *App. Phys. Lett.*, vol. 39, no. 12, pp. 987–989, Dec. 15, 1981.

[20] A. Borghesi, B. Pivac, A. Sassella, and A. Stella, "Oxygen precipitation in silicon," *J. Appl. Phys.*, vol. 77, 1995, Art. no. 4169.
[21] R. C. Newman, "Oxygen diffusion and precipitation in Czochralski silicon," *J. Phys.: Condensed Matter*, vol. 12, pp. R335–R365, 2000.
[22] T. Y. Tan and C. Y. Kung, "Oxygen precipitation retardation and recovery phenomena in Czochralski silicon: Experimental observations, nuclei dissolution model, and relevance with nucleation issues," *J. Appl. Phys*, vol. 59, no. 3, pp. 917–931, Feb. 1, 1986.
[23] S. Zhang, M. Juel, E. Ovrelid, and G. Tranell, "Investigating the effect of carbon on oxygen behavior in n-type Czochralski silicon for PV application," *J Cryst. Growth*, vol. 411, pp. 63–70, 2015.
[24] J. Vanhellemont and C. Claeys, "A theoretical study of the critical radius of precipitates and its application to silicon oxide in silicon," *J. Appl. Phys.*, vol. 62, no. 9, pp. 3960–3967, Nov. 1, 1987.
[25] V. V. Voronkov and R. Falster, "Nucleation of oxide precipitates in vacancy-containing silicon," *J. Appl. Phys.*, vol. 91, no. 9, pp. 5802–5810, May 1, 2002.
[26] B. Sopori *et al.*, "Flash annealing: A method for wafer-level processing of Si substrates to improve their material quality and extend ingot yield for very high efficiency solar cells," to be published.
[27] S. M. Hu, "Effects of ambients on oxygen precipitation in silicon," *Appl. Phys. Lett.*, vol. 36, no. 7, pp. 561–564, Apr. 1, 1980.
[28] G. A. Hawkins and J. P. Lavine, "The effect of rapid thermal annealing on the precipitation of oxygen in silicon," *J. Appl. Phys.*, vol. 65, no. 9, pp. 3644–3654, May 1, 1989.
[29] B. Sopori *et al.*, "Some challenges in making accurate and reproducible measurements of minority carrier lifetime in high-quality Si wafers," in *Proc. 40th IEEE Photovoltaic Spec. Conf.*, 2014, pp. 649–654.
[30] J. D. Murphy, K. Bothe, R. Krain, V. V. Voronkov, and J. Falster, "Parameterisation of injection dependent lifetime measurement in semiconductors in term of Shockley-Read-Hall statistics: An application to oxide precipitates in silicon," *J. Appl. Phys.*, vol. 111, 2012, Art. no. 113709.
[31] J. D. Murphy *et al.*, "The effect of oxide precipitates on minority carrier lifetime in n-type silicon," *J. Appl. Phys.*, vol. 118, 2015, Art. no. 2015706.
[32] D. Macdonald, J. Tan, and T. Trupke, "Imaging interstitial iron concentrations in boron-doped crystalline silicon using photoluminescence," *J. Appl. Phys.*, vol. 103, 2008, Art. no. 073710.
[33] D. Macdonald, T. Roth, and P. N. K. Deenapanray, "Doping dependence of the carrier lifetime crossover point upon dissociation of iron-boron pairs in crystalline silicon," *Appl. Phys. Lett.*, vol. 89, 2006, Art. no. 142107.
[34] N. M. Johnson *et al.*, "Characteristic electronic defects at the Si-SiO_2 interface," *Appl. Phys. Lett.*, vol. 43, 1983, Art. no. 563.
[35] E. H. Poindexter, G. J. Gerardi, M. E. Rueckel, N. M. Johnson, and D. K. Biegelsen, "Electronic traps and Pb centers at Si/SiO2 interface: Band gap energy distribution," *J. Appl. Phys.*, vol. 56, 1984, Art. no. 2844.
[36] J. M. Hwang and D. K. Schroder, "Recombination properties of oxygen precipitated silicon," *J. Appl. Phys.*, vol. 59, 1986, Art. no. 2476.

Authors' photographs and biographies not available at the time of publication.